Construction and Building Materials 205 (2019) 39–51

Contents lists available at ScienceDirect

Construction and Building Materials

journal homepage: www.elsevier.com/locate/conbuildmat

Properties of lightweight concrete made with core-shell structured lightweight aggregate

Feras Tajra [a], Mohamed Abd Elrahman [a,b], Christian Lehmann [a], Dietmar Stephan [a,*]

[a] Department of Building Materials and Construction Chemistry, Technische Universität Berlin, Germany
[b] Department of Structural Engineering, Mansoura University, Egypt

HIGHLIGHTS

- Core-shell structured lightweight aggregate (CSA) was produced by cold bonding method.
- Effects of curing method and surface treatment on properties of CSA were investigated.
- CSA and expanded clay aggregate (ECA) were used for production of lightweight concrete.
- Mechanical and durable Properties of concrete made of either CSA or ECA were compared.

ARTICLE INFO

Article history:
Received 9 October 2018
Received in revised form 15 January 2019
Accepted 27 January 2019
Available online 6 February 2019

Keywords:
Cold-bonded lightweight aggregate
Surface treatment
Lightweight aggregate concrete
Mechanical behavior
Thermal conductivity
Durability

ABSTRACT

In this study, core-shell structured lightweight aggregates (CSA) were produced through the cold bonding method, by encapsulating an expanded perlite particle (as a core structure) within a shell matrix composed of cement, fly ash and expanded perlite powder. The effect of different curing regimes on the mechanical and microstructural properties of the CSA were studied. To enhance the characteristics of the aggregates produced, they were surface treated by a mixture of cement and silica fume, using two different treatment methods. Afterwards, the properties of lightweight concrete made of either CSA or expanded clay aggregate (ECA) were compared closely in terms of their potential economic and environmental benefits, in response to the high energy consumption associated with the production of ECA. The results revealed that curing at a relative humidity of 99% is the most appropriate curing method for CSA. In addition, treating the CSA surface contributes significantly to enhancing its bulk crushing strength, by about 14–18%. The findings also demonstrate the feasibility of using CSA to produce lightweight aggregate concrete, with a dry density and compressive strength ranging from 1115 to 1540 kg/m^3 and from 17.9 to 25.8 MPa, respectively, with a corresponding thermal conductivity range of 0.3169–0.6660 W/m·K.

1. Introduction

Lightweight aggregate concrete (LWAC) has recently attracted great interest and large industrial demand in a wide range of construction projects [1,2]. LWAC has lower density and thermal conductivity than conventional concrete and offers many technical, economic and environmental advantages [3,4]. Compared to normal-weight concrete (NC), LWAC is made either by replacing all normal-weight aggregates, or only the coarse fraction, with lightweight aggregates (LWAs), which can be natural or artificial [5]. Due to the depletion of natural resources, particular attention has been paid to the utilization of artificial LWAs produced either by sintering or by cold bonding method.

Sintered LWAs such as expanded clay (Liapor and Leca) and expanded glass (Poraver and Liaver), produced at a temperature of about 1200 °C, are widely utilized because of their very low density and good mechanical properties [6]. Yu et al. [7] have used LWAs manufactured from recycled glass to produce ultra LWAC with a dry density range of 650–700 kg/m^3 and a corresponding compressive strength of 8–12 MPa. Lo Yu et al. [8] have produced LWAC with a 28-day compressive strength of 29–43 MPa and a density of 1617–1850 kg/m^3, using normal-weight sand and expanded clay coarse aggregate.

Compared with sintering method, cold bonding method is characterized by minimal energy consumption and lower pollutants emission [9]. Moreover, being the aggregates occupy about

* Corresponding author.
E-mail address: stephan@tu-berlin.de (D. Stephan).

https://doi.org/10.1016/j.conbuildmat.2019.01.194
0950-0618/

65–75% of the total volume of concrete [10], cold bonding method can be considered a great opportunity for converting different and an enormous amount of waste and by-product materials into added value product. Therefore, many studies in recent years have concentrated on the behavior of LWAC made of cold-bonded produced with different waste materials [11–15].

However, although the performance of cold-bonded LWAC has been demonstrated, little attention has been paid to emulating the performance of LWAC produced with sintered LWAs available in the market; the main reason for this could be the high density of cold-boned LWAs, as compared to that of sintered ones. Therefore, a new cold-bonded method was developed in previous study to produce core–shell structured LWA with low density as a potential construction material for the production of lightweight aggregate concrete. The production process, as well as the properties of core–shell LWA (CSA), have been exhaustively explained and studied in [16].

In this study, the practical applications of CSA in the production of LWAC are studied deeply by evaluating the mechanical and durability behavior of CSA concrete, in comparison with ECA concrete, aiming to increase the use of cold-bonded LWAs, which may have a positive impact from an environmental and economic perspective.

2. Experimental program

This research was divided into two phases. The first phase consisted of producing CSA by the encapsulation of expanded perlite particles, within a cover matrix composed of cement, fly ash and expanded perlite powder. Being that this kind of aggregate is new, two necessary investigations were performed as an important step toward studying its practical applications in concrete. The scope of these investigations covered two different aspects: (1) determining the effects of different curing methods on the properties of the aggregate produced, to choose and employ the most appropriate curing process; (2) treating the aggregate surfaces with a cement-silica fume mixture for the purposes of enhancing their properties. The second phase of the experimental work was extensively carried out in regard to the feasibility of using CSA for the production of LWAC. The behavior of CSA concrete was studied and compared with concrete produced with expanded clay aggregates, in terms of mechanical properties and durability.

2.1. First stage

2.1.1. Raw materials and the production of CSA

As demonstrated in detail in a previous study [16], a pelletizer disc of 40 cm diameter and 10 cm depth was used and operated at an angle of 35° and a speed of 30 rpm. To produce CSA, expanded perlite particles (EP) were encapsulated in a shell structure composed of 18 vol% ordinary Portland cement (OPC, CEM I 42.5R), 49 vol% class F fly ash (FA) and 33 vol% expanded perlite powder (EPP), with a particle size <125 μm. Two different sized fractions of CSA, 2–4 and 4–8 mm, were manufactured by using 1–2 and 2–4 mm perlite particles as cores, respectively. The particle size distributions of the raw materials are shown in Fig. 1. The physical and chemical properties of OPC, FA and EPP are presented in Table 1.

2.1.2. The effects of curing methods on the strength development of CSA

Cold-bonded LWAs require an appropriate curing regime and a sufficient curing period to achieve enough strength to be put into practice [17,18]. In this investigation, to identify the suitable curing method for the CSA, three different practical methods were applied: under water (UW), under a controlled relative humidity of 65% (RH 65%) and under a controlled relative humidity of 99% (RH 99%). These curing methods were applied at a temperature of 20 ± 1 °C until the day of testing. Since the strength of LWAs has a considerable impact on the properties of LWAC [19,20], the bulk crushing strength of CSA, subjected to different curing methods, was closely studied. It was tested according to EN 13055, Annex C [21], using a steel test cylinder, 113 mm in diameter and 100 mm in height. The bulk crushing strength was measured by dividing the force, recorded at 20 mm of compression for 100 s, by the specimen area. This investigation was performed on oven-dried CSA with a size range of 4–8 mm. Three aggregate samples of each curing method were tested, and the mean value was taken into consideration.

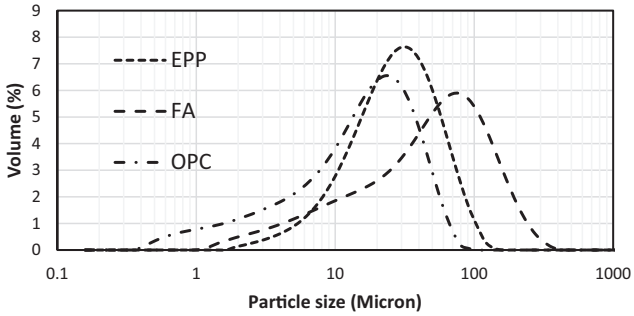

Fig. 1. Particle size distributions of OPC, FA, and EPP.

The results in Fig. 2 show that, up to an age of 28 days, an increase in curing duration resulted in a significant increase in the crushing strength. All the aggregates gained about 75% of their 28-day strength within 7 days, exhibiting a further marginal improvement in their crushing resistance when the curing period was extended to 56 days. A maximum crushing strength of 3.13 MPa was achieved by the aggregate cured at RH 99%, whereas the aggregate cured at RH 65% showed the lowest strength, of 2.12 MPa. Compared with the UW curing method, the RH 99% method enhanced the crushing strength by about 17%, while it decreased by about 29%, 26% and 21% at an age of 7, 28 and 56 days, respectively, when RH of 65% was applied. This evaluation shows that curing at RH 99% is more beneficial than the other methods for the crushing strength enhancement of CSA. This tendency will be explained and discussed deeply in the following investigations.

2.1.3. The effects of curing methods on the microstructural characteristics of CSA

In this aspect, thermogravimetric analysis (TGA), X-ray diffraction (XRD) and SEM tests were performed on the cover matrix of the aggregate produced to justify why the aggregate cured at RH 99% possessed higher crushing strength than that cured under water and at RH 65%. To perform the XRD and TGA tests, the aggregate sample was firstly dried in an oven at 105 °C until reaching a constant weight, after removing the perlite core, the cover matrix was ground and used for the tests.

2.1.3.1. Thermogravimetric analysis (TGA). Fig. 3a and 3b show the thermogravimetric analysis of the aggregate under different curing methods, at an age of 7 and 56 days, respectively. Calcium hydroxide content was calculated based on the mass loss due to decomposition of $Ca(OH)_2$, between 400 and 500 °C [22], using the following equation:

$$CH = W_{CH} \times \frac{74}{18} \quad (1)$$

Table 1
The chemical and physical properties of OPC, FA, and EPP.

Material (wt%)	CaO	SiO_2	Al_2O_3	Fe_2O_3	MgO	Na_2O	K_2O	Loss on ignition	Specific density (g/cm^3)
OPC	64.2	18.8	5.1	3.3	1.8	0.1	0.9	3.05	3.11
FA	4.4	55.9	22.6	6.7	1.9	0.8	1.9	2.50	2.34
EPP	0.9	76.9	11.3	0.9	0.1	3.6	3.6	1.02	2.38

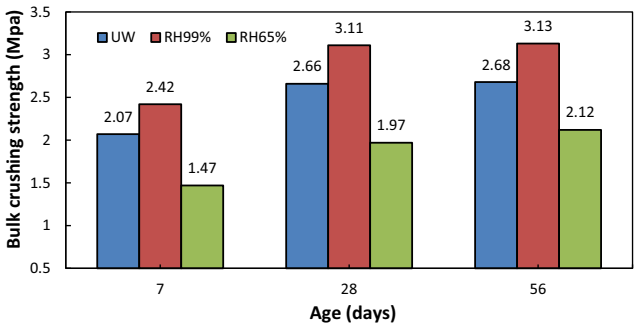

Fig. 2. Bulk crushing strength development.

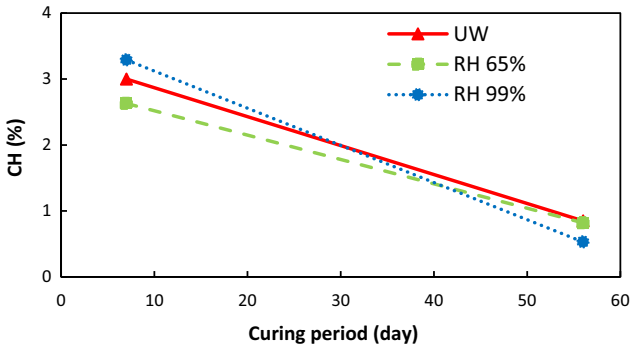

Fig. 4. Calcium hydroxide content under different curing methods and ages.

Where: W_{CH} is the mass loss due to the evaporation of water between 400 and 500 °C, 74 and 18 are the molecular masses of calcium hydroxide and water (g/mol), respectively.

It was noticed that, from the calculated values of CH content (Fig. 4), at an age of 7 days the aggregates cured at RH 99% exhibited the highest CH content, followed by those cured under water and finally those cured at RH 65%. As the hydration of OPC produces about 15–25 wt% of calcium hydroxide (CH) [23], the CH content at an early age of a cement-pozzolan system indicates the extent of cement hydration; therefore, at an age of 7 days, a high degree of cement reaction, associated with the highest quantity of CH and highest crushing strength, might have been caused by curing at RH 99%. Alternatively, after 28 days, the pozzolanic reaction starts by consuming the available CH, converting it into more hydration products [14]. Therefore, at an age of 56 days, less CH content can be considered as an indicator of a high pozzolanic reaction rate and thus more formation of C-S-H phases associated with higher strength. This correlation is clearly demonstrated at an age of 56 days, where the findings in Figs. 3 and 4 show an obvious inverse relation between the CH content and the crushing strength. Consequently, it can be concluded that among the curing methods studied, curing at RH 99% effectively enhances the reaction in the cover matrix of CSA, thus improving its bulk crushing strength.

2.1.3.2. X-ray diffraction (XRD). The correlation between TGA analysis and crushing strength results was further proved by observing the intensity of the CH peak from XRD analysis. Consideration of the CH peak, located at around the two theta angle of 18°, is the key performance indicator for a cement-pozzolan system [24]. As evident in Fig. 5a, the 7-day-old CSA cured at RH 99% showed the highest CH peaks, followed by that cured under water and then by that cured at RH 65%. The highest CH peak can be a consequence of a high rate of cement hydration accompanied by more C-S-H. Curing at RH 99% therefore resulted in a significant increase in the crushing strength of CSA, compared to the other curing methods. The XRD patterns of 56-day-old CSA in Fig. 5b, indicate that the intensity of CH peaks decreased significantly with an increase

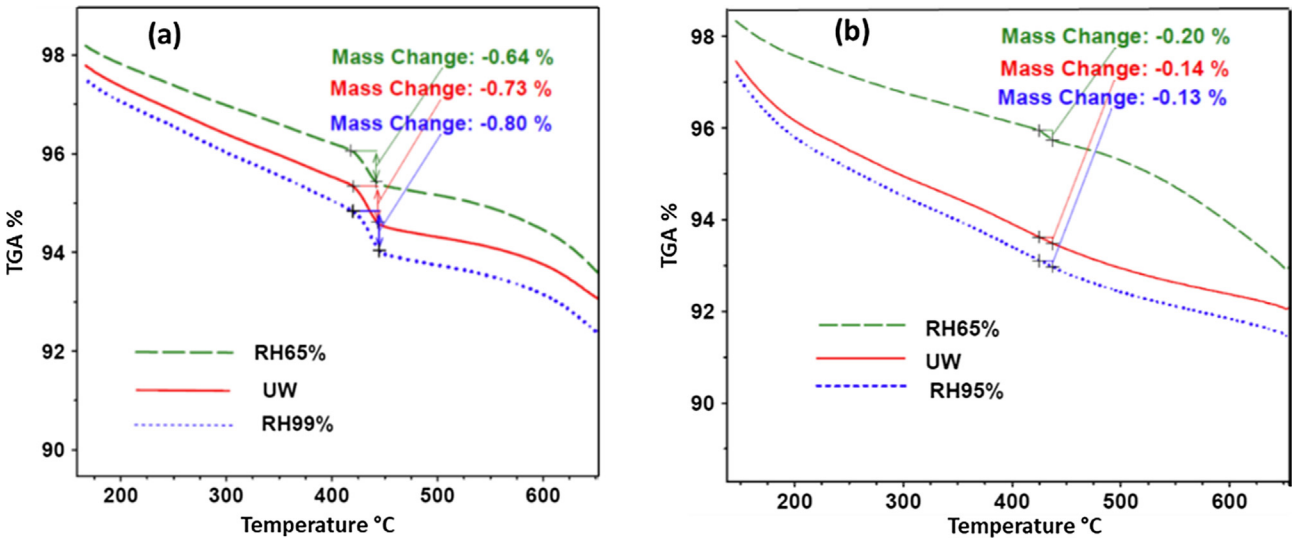

Fig. 3. TGA results of CSA under different curing methods at a) 7 days, b) 56 days.

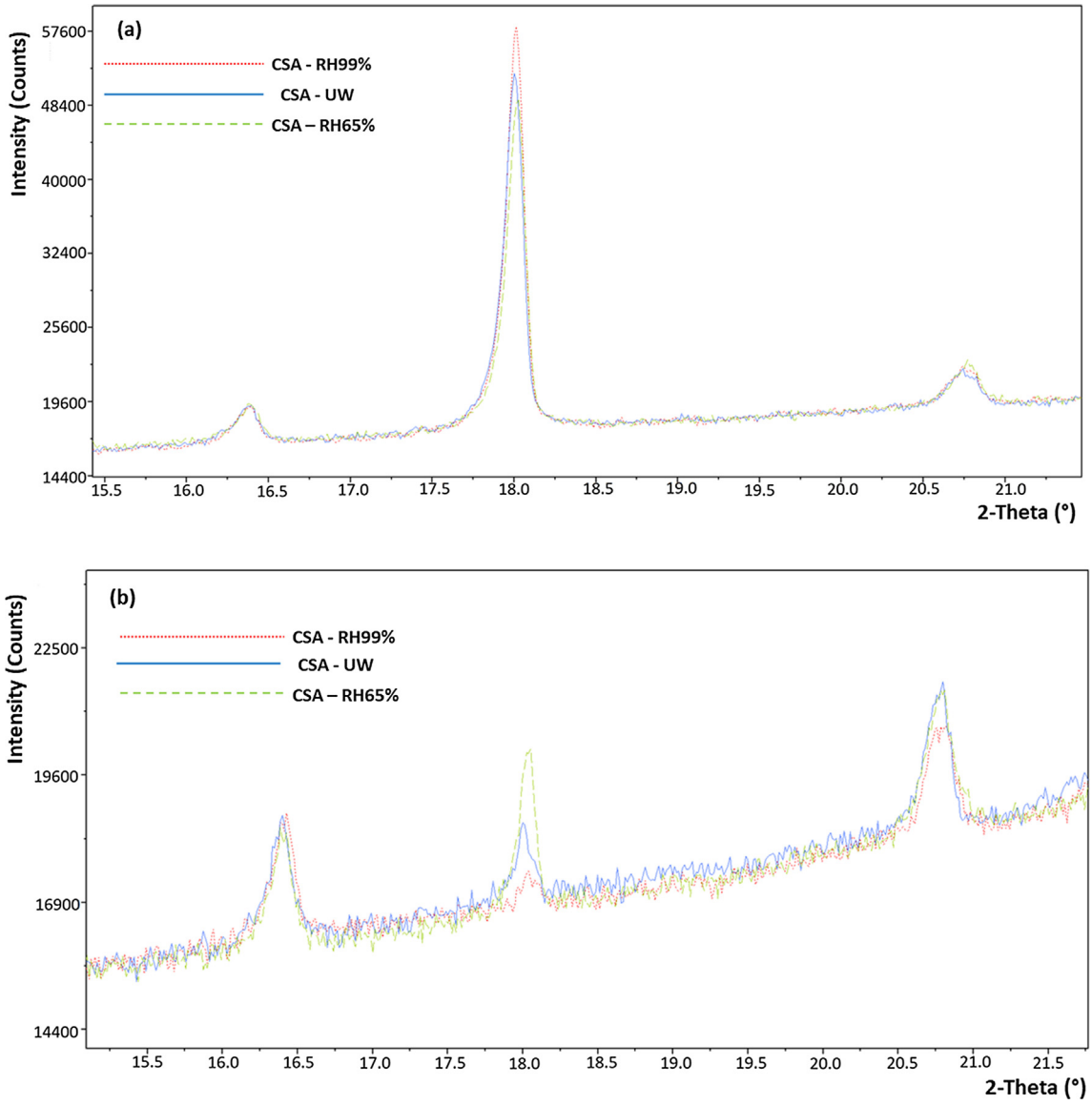

Fig. 5. XRD results of CSA under different curing methods; (a) at 7 days and (b) at 56 days.

in the curing period. This is attributable to the pozzolanic reaction, as mentioned before. It can be noticed from Fig. 5b, that the CSA cured at RH 99% exhibited the lowest CH peak, which can be explained by the high pozzolanic reaction rate achieved with this method.

2.1.3.3. Scanning electron microscopy (SEM). The microstructures of 7 and 56-day-old CSA are shown in Figs. 6 and 7, respectively, with a noticeable microstructural difference between the differently cured aggregates being visible. At an age of 7 days, the microstructures of CSA cured at RH 65% and under water (Fig. 6a and b) were porous. Only a low amount of hydration products, on the surface of fly ash particles, can be seen in the CSA cured at RH 65% (Fig. 6a), with the microstructure of CSA cured under water (Fig. 6b) being somewhat denser, due to the formation of more hydration products. These observations denote a relatively low stage of cement hydration achieved by these two methods. Conversely, in the case of CSA cured at RH 99% (Fig. 6c), the availability of a high concentration of CH, which later takes part in the pozzolanic reaction, is a sign of a high degree of cement hydration.

After 56 days of curing, the presence of CH and ettringite in Figs. 7d and 7e can be explained by a relatively low pozzolanic reaction rate, caused by curing at RH 65% and under water. At the same time, the absence of CH crystals, which were consumed and converted into more hydration products (Fig. 7f), confirm that the pozzolanic reaction sped up when the RH 99% method was applied. Accordingly, it can be concluded that curing at RH 99% resulted in an increase in the rate of cement and pozzolanic reaction in the cover matrix of the CSA, which is consistent with its high crushing strength, as compared with the CSA cured under water and at RH 65%.

2.1.4. The effects of surface treatment on CSA properties

The high water absorption of LWAs negatively affects the mechanical and durability performance of LWAC [25]. Many researchers have reported that surface treatment of lightweight aggregate substantially decreases its water absorption while enhancing its mechanical properties [14,26]. In the present study, the manufactured aggregates with a size range of 4–8 mm were surface-treated by a cement-silica fume mixture, using two different methods. A schematic diagram of the CSA cross section is pre-

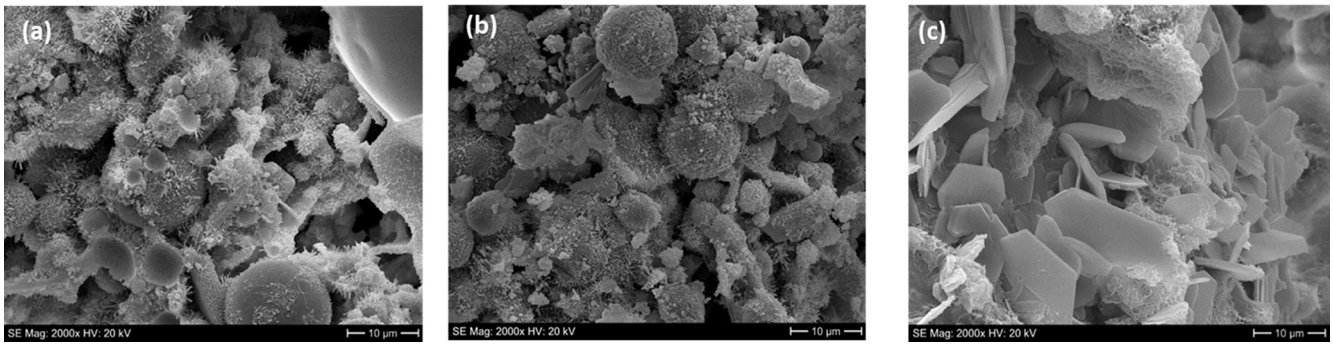

Fig. 6. SEM images of CSA at age of 7 days cured at; (a) RH 65%, (b) UW, (c) RH 99%.

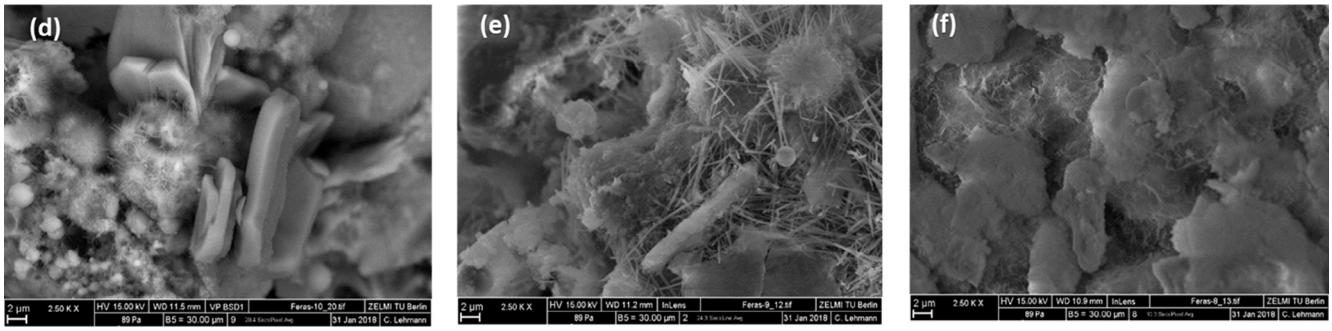

Fig. 7. SEM images of CSA at age of 56 days cured at; (d) RH 65%, (e) UW, (f) RH 99%.

sented in Fig. 8. After producing the CSA, the fresh pellets were kept in sealed bags for 24 h, after which they were treated either by a cement-silica fume slurry, or by coating with a thin film of cement-silica fume. In the first method, the slurry was made of 90 wt% OPC, 10 wt% silica fume (SF) and a water/powder ratio of 1.2. The aggregate was immersed in the slurry for 30 min and then sieved to filter out the excess slurry. Thereafter, the treated aggregate was spread over a mesh to avoid particle-particle cohesion and cured at RH 99%, until the date of testing. However, in the second method, the aggregates were first soaked in water for 5 min, after which the water was totally filtered out. The saturated particles were introduced into the pelletizer disc, which was rotated at a speed of 15 rpm. Next, cement-silica fume powder mixture composed of 90 wt% OPC and 10 wt% SF was sprayed on the particle surfaces. Afterwards, the treated samples were removed from the pelletizer and cured at RH 99%, until the date of testing.

The optical microscope images in Fig. 9 clearly show the shape and cross section of ECA. As it is known, ECA is prepared by heating clay at a temperature of 1200 °C, the high temperature inciting the clay to expand to several times its original size and to form spherical pellets with a very highly porous structure [27]. Fig. 9 also shows the shape and cross section of the CSA. Compared with non-treated CSA, the slurry treatment led to the formation of an irregular layer on the particle surface. Moreover, the cross section of the slurry-treated particle clearly indicates the inefficiency of this method to completely cover the whole surface of the particle. In contrast, the nearly spherical shape of the CSA particle was maintained by the application of a coating treatment, performed using the pelletizer disc. This method enabled the powder mixture to be uniformly distributed on the whole surface of the particle, covering it with a thin uniform film of approximately 300 µm thickness, as shown clearly in Fig. 9.

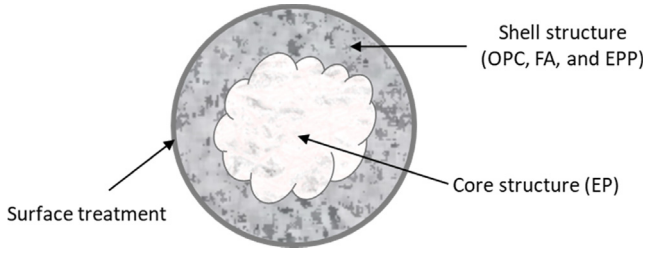

Fig. 8. Schematic diagram of the pellet cross section.

After 28 days of curing at RH 99%, the effect of the surface treatment was evaluated through the physical and mechanical properties of the treated and non-treated CSA. The physical properties were measured in terms of water absorption, oven-dry (OD) particle density and loose bulk density, in accordance with EN 1097-6 [21] and EN 1097-3 [28]. These tests were performed on three samples of each aggregate type, and the average value was taken into evaluation. The manufactured aggregates were coded in Table 2 as: CSA for non-treated aggregates as a control sample; CSA.SL and CSA.CO for slurry-treated and coating-treated aggregates, respectively.

The results in Table 2 indicate that the cold bonding technique can be successfully employed to produce CSA with a low particle and loose bulk density of 0.98 g/cm^3 and 549 kg/m^3, respectively, with a corresponding crushing strength of 3.11 MPa. Compared to CSA, as a control specimen, the particle density increased slightly from 0.98 to 1.00 g/cm^3, while water absorption decreased marginally from 44 to 42 wt%, when the slurry treatment was applied. This insignificant effect is attributable to the inability of this method to secure full cover on the particle surface. Moreover, this method resulted in the formation of protrusions on the surfaces of the aggregates, as shown in Fig. 9. These protrusions contributed to weakening the filling ability of the CSA.SL, thus decreasing both the loose bulk density and bulk crushing strength, as illustrated in Table 2. In contrast, the coating treatment method

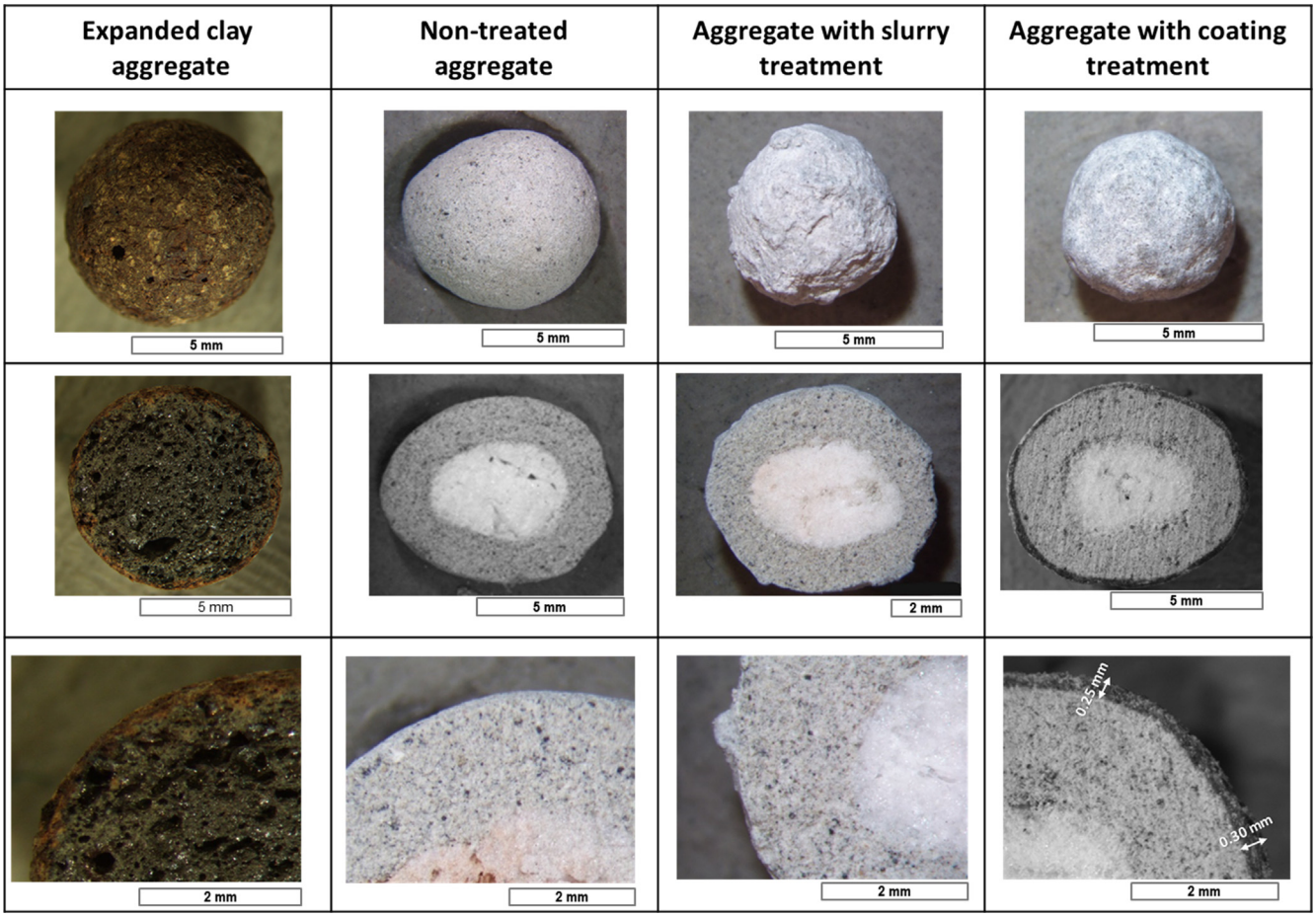

Fig. 9. Microscopy images of ECA, treated and non-treated CSA.

Table 2
Physical and mechanical properties of treated and non-treated CSA.

Type of CSA	Particle density g/cm^3	Loose bulk density kg/cm^3	Water absorption wt.-%	Bulk crushing strength MPa
CSA	0.98	549	44	3.11
CSA.SL	1.00	540	42	2.77
CSA.CO	1.11	608	32	3.55

resulted in a marked improvement in the physical and mechanical properties of the aggregate produced. The particle density, loose bulk density and bulk crushing strength of CSA.CO increased by about 13%, 11% and 14%, respectively, compared with CSA. In addition, the formation of a dense thin film on the aggregate surface effectively decreased water absorption by about 27%. Consequently, it can be concluded that the coating treatment achieved a good efficiency, resulting in a stronger and much more impermeable shell structure, as shown by the higher bulk crushing resistance and lower water absorption, as compared with the non-treated aggregates.

Based on the results of the first stage, it was decided to use the RH 99% curing condition and the coating surface treatment, to produce the aggregates for the second stage of the research.

2.2. Second stage

In this part, a large quantity of CSA with a size range of 2–4 and 4–8 mm was produced and treated by the coating method as described above, the aggregates then cured at RH 99% for 28 days. Afterwards, the applicability of these kinds of LWAs for the production of lightweight aggregate concrete was studied in detail.

2.2.1. Raw materials and production of lightweight aggregate concrete

A total of six lightweight concrete mixtures were prepared and tested. In all the mixes, a binder content of 450 kg/m^3, composed of 90 wt% OPC and 10 wt% SF and a water/binder ratio of 0.36 were used. The mixes were divided into two groups, differing in terms of the type of fine aggregate used. Natural quartzite sand (NS) and lightweight expanded clay sand (ECS) were utilized to produce the mixes of groups 1 and 2, respectively. Furthermore, expanded clay aggregate (ECA), non-treated CSA and surface-treated CSA (CSA.ST) were used as a coarse LWA. To study only the effects of aggregate type on concrete properties, the particle size of all aggregate types was controlled by sieving; 0–2 mm for the fine fraction and 2–4 and 4–8 mm for the coarse fraction. The physical and mechanical properties of the aggregates used are presented in Table 3. To eliminate the effects of aggregate water absorption on the properties of the fresh concrete, the LWAs were immersed in water before mixing and used in a saturated surface-dry condi-

Table 3
Physical and mechanical properties of coarse and fine aggregates.

Type of LWAs	Size of LWAs	Particle density		Bulk density	Water absorption	Bulk crushing strength
		SSD*	OD**			
mm		g/cm^3		kg/cm^3	wt%	MPa
ECA	4–8	0.70	0.51	310	35	1.44
ECA	2–4	0.74	0.61	345	23	2.08
ECS	0–2	1.60	1.17	620	37	–
NS	0–2	2.65	2.6	1650	0.5	–
CSA	4–8	1.41	0.98	549	44	3.11
CSA	2–4	1.44	1.00	566	43	3.54
CSA.ST	4–8	1.48	1.11	608	32	3.55
CSA.ST	2–4	1.50	1.10	622	36	4.20

* Saturated surface-dry.
** Oven-dry.

tion (SSD), as recommended in [29,30]. Polycarboxylic ether superplasticizer (PCE), with a density of 1.08 g/cm^3 was used to achieve reasonable consistency. A viscosity modifying admixture was utilized as a stabilizer to prevent concrete segregation. Table 4 presents the mix proportions of the concrete mixtures, labeled by aggregate type as ECA-NS, CSA-NS and CSA.ST-NS for group 1 and as ECA-ECS, CSA-ECS and CSA.ST-ECS for group 2. The fresh concrete was cast into 100 mm cubical steel molds and 100 mm·200 mm cylinder molds, in accordance with EN 12390-1 [31]. The specimens were covered with a polyethylene sheet to avoid evaporation and then demolded after 24 h and cured at a relative humidity of 99%, until the testing day.

2.2.2. Test methods

The consistency of the fresh concrete was measured using a flow table test, according to EN 12350-5 [32]. The dry density and compressive strength tests of 100·100·100 mm^3 specimens were conducted as specified in EN 12390-7 [33] and EN 12390-3 [34], respectively. A modulus of elasticity test was performed on 100·200 mm cylinder specimens, in accordance with EN 1048-5 [35]. The thermal conductivity of 100 mm oven-dried cube samples was evaluated via the Hot Disk device, model TPS 2200, as shown in Fig. 10.

The durability of LWAC was investigated by means of capillary water absorption and water penetration tests. The capillary suction of water was evaluated according to EN ISO 15148 [36], as shown in Fig. 11a. The specimens were first dried at 105 °C, until a constant weight was achieved. The side surfaces of the specimen were then coated by a paraffin layer, to ensure unidirectional absorption. Afterwards, the concrete specimens were placed in a container, which was partially filled with water at a level of 5 mm above the bottom of the specimen. The weight gain due to the capillary water absorption was measured at several times intervals:

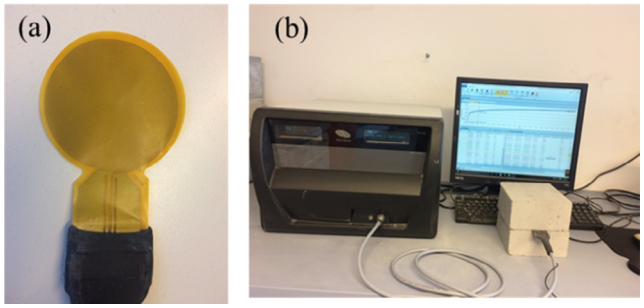

Fig. 10. Thermal conductivity test: (a) Hot Disk sensor; (b) sensor with a specimen.

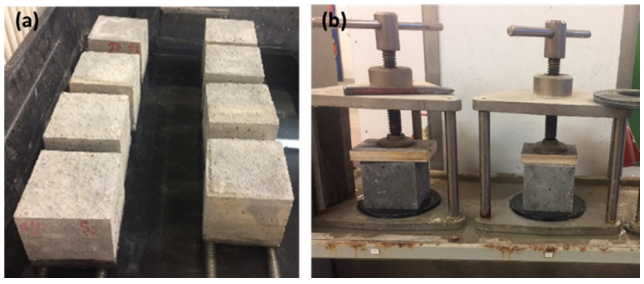

Fig. 11. Durability tests: (a) capillary water absorption; (b) water penetration.

20 min, 1, 2, 3, 4, 5, 6, 7, 8 and 24 h. The capillarity coefficient was calculated using the following equation:

$$K = \frac{\Delta m_{tf} - \Delta m_0}{\sqrt{t_f}} \quad (2)$$

Table 4
Mix proportions of concretes (kg/m^3).

Group	1			2		
Mix No.	M1	M2	M3	M4	M5	M6
Mix ID	ECA-NS	CSA-NS	CSA.ST-NS	ECA-ECS	CSA-ECS	CSA.ST-ECS
w/b	0.36	0.36	0.36	0.36	0.36	0.36
Silica fume	45	45	45	45	45	45
Cement	405	405	405	405	405	405
Water	162	162	162	162	162	162
Superplasticizer	4.4	4.4	4.4	4.4	4.4	4.4
Stabilizer	0.4	0.4	0.4	0.4	0.4	0.4
Coarse aggregate 4–8 mm*	170	348	362	170	348	362
Coarse aggregate 2–4 mm*	119	228	237	119	228	237
Sand 0–2 mm*	593	593	593	365	365	365

* Saturated surface-dry condition.

Where: K is the capillarity coefficient kg/(m^2·h$^{0.5}$), Δm_0 and Δm_{tf} are the amounts of water absorbed per unit area (kg/m^2) at 0 and 24 h respectively and t_f is the testing period (h).

The water penetration test was performed in accordance with DIN EN 12390-8 [35], as shown in Fig. 11b, by applying 1 bar water pressure for 72 h, and then measuring the water penetration depth. All the aforementioned investigations were carried out on three concrete samples of each mix and the mean value was considered.

Furthermore, SEM was also performed on the concrete specimens to evaluate the interfacial transition zone between the aggregate and the cement matrix. The sample prepared for the SEM test is shown in Fig. 12.

3. Results and discussion

The measured flow diameter of the fresh concrete mixtures ranged from 42 to 45 cm, which classifies them as type F3, according to EN 206-1 [37]. It is clear from the slump flow of fresh concrete (Fig. 13) that no segregation or bleeding occurred in the concrete mixtures. In addition, as can be seen in Fig. 14a, b and c, the CSA, ECA and CSA.ST maintained their original shape, without apparent damage, which denotes that the aggregates had enough strength to avoid the probable crushing caused by the mixing of concrete.

3.1. Physical and mechanical properties evaluation

The aim of this study was to evaluate the physical and mechanical properties of LWAC made with treated and non-treated CSA, compared with LWAC produced with expanded clay aggregate. Considering the mixes of group 1, produced with NS, the replacement of ECA in M1 with CSA (M2) resulted in an approximately 15% and 13% increase in dry density and compressive strength, respectively. M2 therefore presented a slightly lower strength/density ratio than M1, as shown in Fig. 15c. In contrast, as shown in Fig. 15a and b, M3 produced with CSA.ST showed a compressive strength of 29.1 MPa, associated with a dry density of 1540 kg/m^3; values which are higher than that of M1 by about 19 and 27%, respectively. The use of CSA.ST in M3 therefore leads to concrete with a strength/density ratio of 18.90, which is higher than that of M1 and M2. Interestingly, in comparing M2 (CSA-NC) and M3 (CSA.ST-NC), aggregate surface treatment contributed strongly to enhancing concrete strength by about 13%, from 25.8 to 29.1 MPa, despite its marginal effect on concrete density. This is mainly attributable to the crushing strength of CSA.ST, which is higher than that of CSA, as was shown above in Table 3. This evaluation confirms that the strength of LWAC is mainly affected by aggregate strength [38,39].

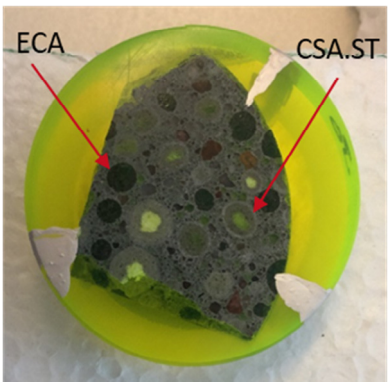

Fig. 12. Sample prepared for SEM test.

Fig.13. Flow table test according to EN 12350-5.

The results of tests performed on concretes produced with expanded clay sand (group 2) show the same trend as those produced with NS. Compared to M4, replacing ECA by CSA.ST in M6 increased both the density and strength of concrete by about 26% and 42%, respectively. A marked increase in strength/density ratio was therefore also observed in Fig. 15c. Consequently, it can be emphasized that the surface treatment of CSA, described herein, is a convenient technique for enhancing concrete strength without a strong impact on its density.

Moreover, Fig. 16 indicates a strong correlation between the dry density and the compressive strength of the concrete produced, with a correlation coefficient R^2 of 0.9463. However, the results show that the dry density and compressive strength of concretes produced with treated and non-treated CSA ranged from 1115 to 1540 kg/m^3 and from 17.9 to 29.1 MPa, respectively. Therefore, this concrete covers the EN 206-1 LWAC density classes from D1.2 to D1.6. It can also be classified as a structural LWAC, according to its compressive strength [40].

Fig. 17 shows the crushed specimen after performing the compressive strength test. It is clear that both CSA and ECA were broken along their diameter, with the clear emergence of the perlite cores, shown in Fig. 17a, being proof of this. Concrete failure therefore took place in the LWAs, being the weakest ingredient of LWAC [41,42] and not in the interfacial transition zone (ITZ) between the LWAs and the cement matrix. This confirms that the failure of LWAC with a high cement content of more than 350 kg/m^3, usually happens in the LWA and as such, that the strength of LWAC containing a high cement content, is mainly affected by the strength of LWA [43].

The modulus of elasticity of LWAC is affected by the type and volume of the LWAs, as well as by the modulus of elasticity of the cement matrix [44,45]. Generally, the results in Fig. 15d show that the modulus of elasticity increased with the compressive strength of concrete, stemming from the replacement of ECA with CSA. In group 1, the modulus of elasticity increased from 10.85 to 11.75 GPa and from 10.85 to 12.5 GPa, when the ECA was replaced with CSA and CSA.ST, respectively. This is mainly attributable to the crushing strength of the CSA and CSA.ST, which is higher than that of ECA, as shown in Table 3. The possible reason for this might also be the difference in the pore structure of these aggregates, in consideration of the work of Kockal and Ozturan [46], who have reported that the porosity and pore size of LWAs have an impact on their modulus of elasticity, thus influencing the modulus of elasticity of LWAC. The results of modulus of elasticity tests in the mixes of group 2 show the same trend, with significantly lower values than that of those of group 1. This confirms that the cement matrix composition has a strong influence on the modulus of elasticity [47].

Table 5 also shows the estimated values of the modulus of elasticity, in accordance with BS and ACI standards. They were calcu-

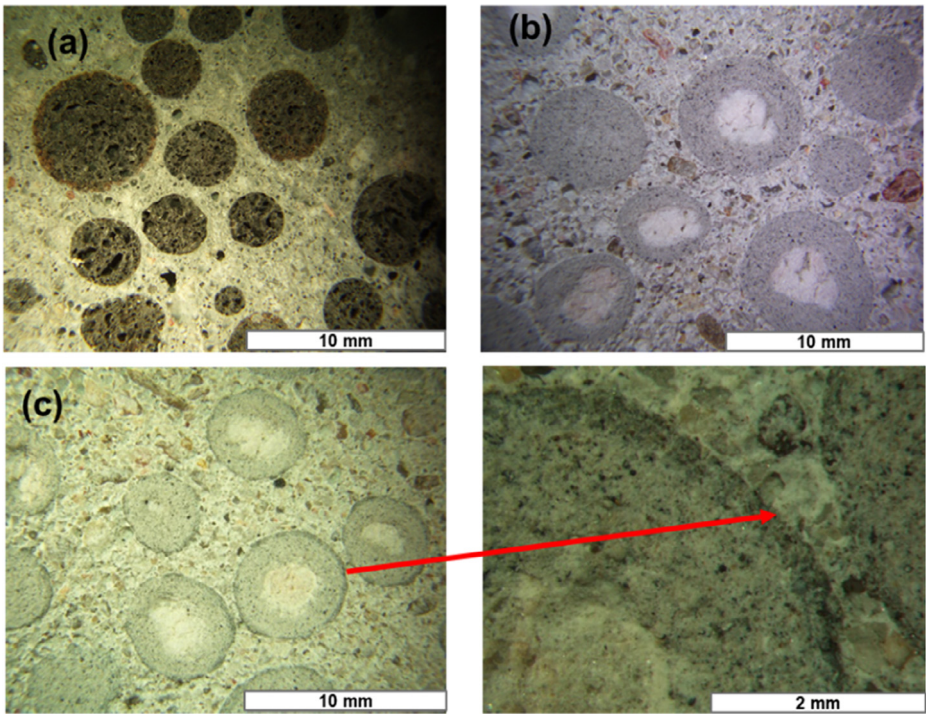

Fig. 14. Cross section of concrete specimens made of ECA (a), CSA (b), and CSA.ST (c).

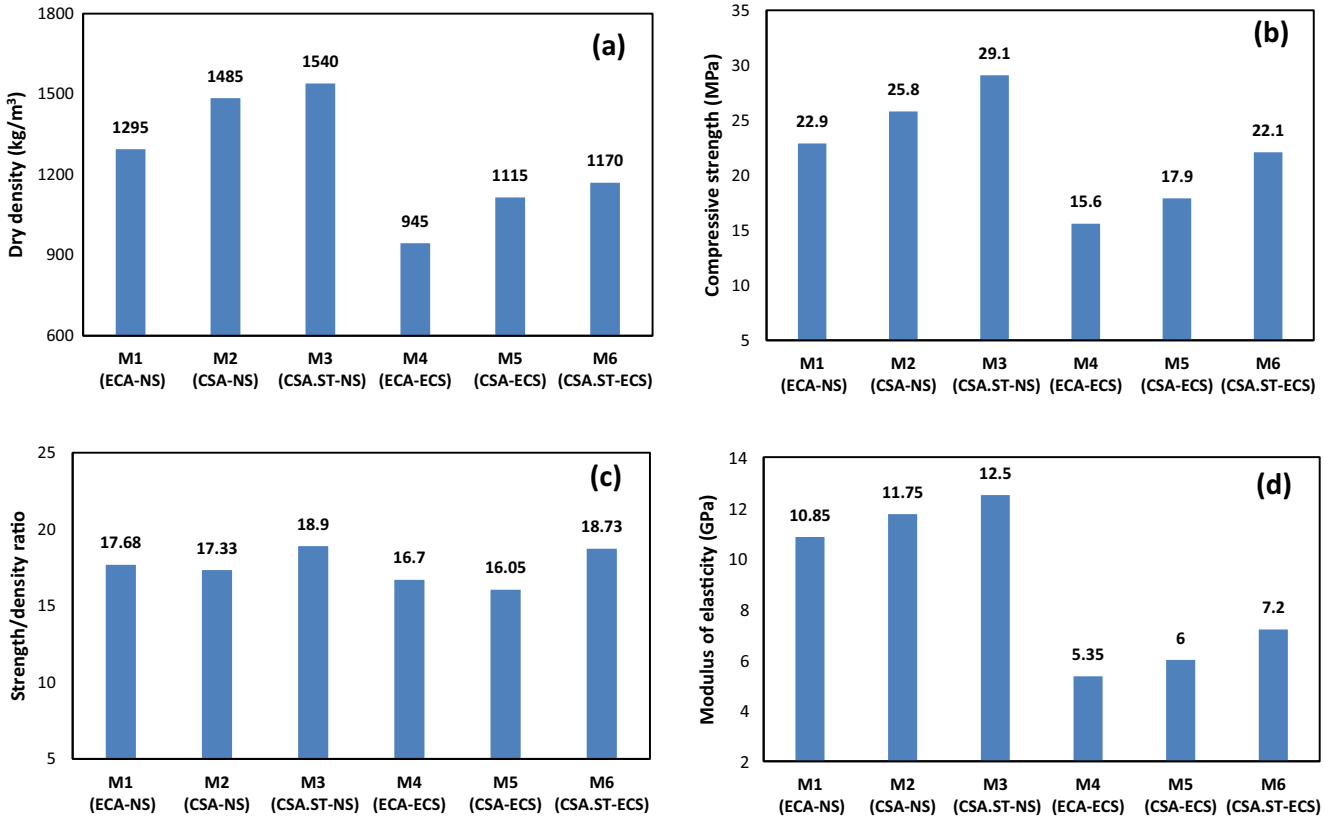

Fig. 15. Properties of LWAC (a) dry density; (b) compressive strength; (c) strength/density ratio; (d) modulus of elasticity.

lated in terms of dry density and cubic compressive strength, using the following equations, as specified in ACI 318 and BS 8110, respectively.

$$E_c = W_c^{1.5} \times 0.043 \times \sqrt{0.8 f_c} \quad (5)$$

$$E_c = W_c^2 \times 0.0017 \times 0.8 f_c^{0.33} \quad (6)$$

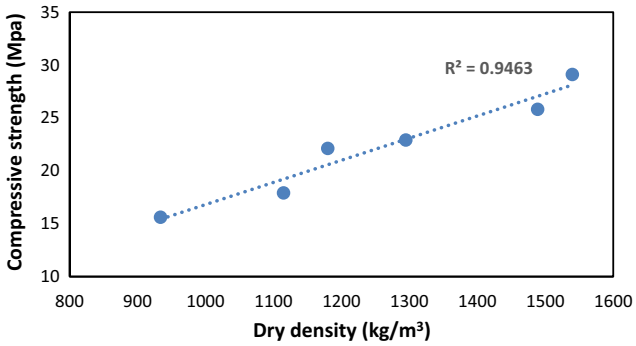

Fig. 16. Relationship between dry density and compressive strength of LWAC.

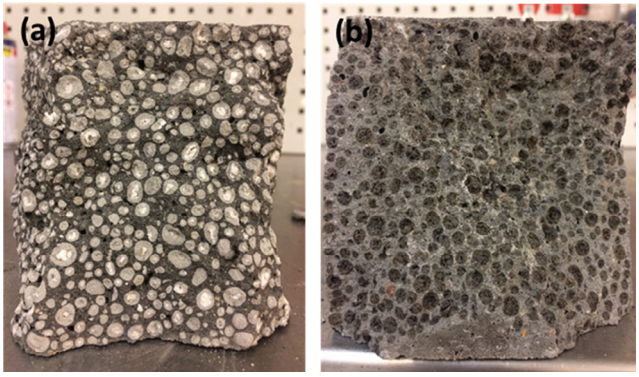

Fig. 17. The distribution of LWAs in concrete: (a) CSA, (b) ECA.

The ratio between the measured and estimated values ranged from 98 to 118% in the mixes made with treated and non-treated CSA. This ratio is located in the typical range of 80–120%, as specified in ACI 318. At the same time, the values measured in the ECA concretes were 123–157 percent of the calculated values. Accordingly, the correlation coefficient R^2, for the values calculated as specified in ACI 318 and BS 8110, decreased from 0.9932 and 0.9962 to 0.9124 and 0.9117, respectively, when the mixes M1 and M4 were included in the analysis, as shown in Fig. 18a and b.

3.2. Thermal conductivity evaluation

Since the aggregate occupies the largest share of the concrete volume, it has a direct and significant influence on the thermal properties of concrete [48]. In this study, the thermal conductivity of the dried concrete was measured via a Hot Disk, as illustrated in Table 6. Compared with M1, thermal conductivity increased by about 39 and 45% when the CSA and CSA.ST were used in M2 and M3, respectively. This is attributable to the highly porous structure and low density of ECA, compared with CSA. Moreover, due to the density of ECS, which is much lower than that of NS, the thermal conductivity of the mixes in group 2, produced using ECS, was significantly lower than those in group 1. A rise in thermal conductivity, of about 6 and 14%, can be observed when ECA was replaced by CSA (M5) and CSA.ST (M6), respectively.

Asadi et al. (2018) [49] have demonstrated a relationship between thermal conductivity (λ) and dry density (ρ), by analyzing 185 results reported in the literature. They have proposed Eq. (7) for calculating the thermal conductivity of concrete, with a density range of 150–2350 kg/m^3.

$$\lambda = 0.0625e^{0.0015\rho} \quad (7)$$

In this study, Fig. 19 represents the relationship between the values measured for dry density and thermal conductivity. It confirms a good correlation between them, with a correlation coefficient R^2 of 0.9476. From this figure, Eq. (8) can be deduced to predict the thermal conductivity of the LWAC produced, being almost the same as Eq. (7):

$$\lambda = 0.064e^{0.0015\rho} \quad (8)$$

3.3. Durability property evaluation

Fig. 20 shows the cumulative increase in specimen mass per unit area (Δm), resulting from water absorption by capillarity. It was determined at 20 min, 1, 2, 3, 4, 5, 6, 7, 8 and 24 h, as a function of the square root of time. Next, the concrete samples' water capillarity coefficient was calculated with Eq. (2), as an average of three different samples for each concrete mix. The results, in Fig. 20, indicate that the type of lightweight aggregate and the composition of the cement matrix had a significant effect on the capillary water absorption of LWAC [50]. Fig. 21 shows that the substitution of ECA (M1) with CSA in M2 increased the capillary suction coefficient of concrete, from 0.33 to 0.48 kg/(m^2·h$^{0.5}$). This is mainly attributable to the water absorption of CSA, which is higher than that of ECA. Interestingly, the water absorption coefficient dropped from 0.48 to 0.34 kg/(m^2·h$^{0.5}$), which is roughly similar to that of M1, when the surface treated CSA was used. A similar trend can be discerned for the mixes of group 2, with a water capillarity coefficient higher than the mixes of group 1, by about 65–70%. The reason for this lies in the very high water absorption of ECS, compared to NS. The results of M2, 3, 5, and 6 confirm the effectiveness of aggregate surface treatment in reducing the water permeability of concrete, thus enhancing its durability.

Furthermore, the effectiveness of aggregate surface treatment on concrete durability was also proved through the water penetration test performed on M1 and M3. Fig. 22a and b show the water penetration depth in the split samples of M1 and M3, respectively. The penetration depth of M1 was 19 mm, whereas M3 exhibited a penetration depth of 16 mm meaning that, although the difference between the water absorption of ECA and CSA.ST was as stated in

Table 5
Experimental and predicted values of modulus of elasticity.

Group	Mix ID	Modulus of elasticity (GPa)			Measured/Estimated ratio (%)	
		Measured value	Estimated values			
			BS 8110	ACI 318	BS 8110	ACI 318
1	M1 (ECA-NS)	10.85	7.44	8.58	146	127
	M2 (CSA-NS)	11.75	10.23	11.22	115	105
	M3 (CSA.ST-NS)	12.50	11.39	12.54	110	100
2	M4 (ECA-ECS)	5.35	3.41	4.34	157	123
	M5 (CSA-ECS)	6.00	5.09	6.06	118	99
	M6 (CSA.ST-ECS)	7.20	6.11	7.33	118	98

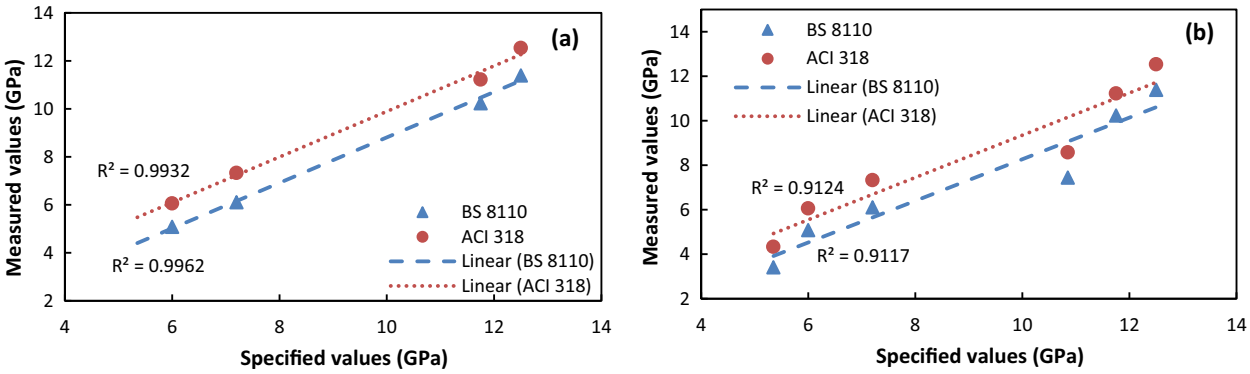

Fig. 18. Relationship between measured and specified values of modulus of elasticity for: (a) M2, M3, M4, and M5; (b) all mixes.

Table 6
Thermal conductivity of LWAC.

Group	Mix ID	Thermal conductivity (W/m·K)
1	M1 (ECA-NS)	0.4578
	M2 (CSA-NS)	0.6364
	M3 (CSA.ST-NS)	0.6660
2	M4 (ECA-ECS)	0.3000
	M5 (CSA-ECS)	0.3169
	M6 (CSA.ST-ECS)	0.3415

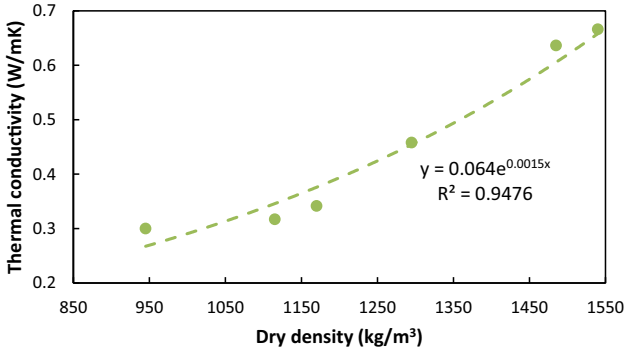

Fig. 19. Relation between dry density and thermal conductivity.

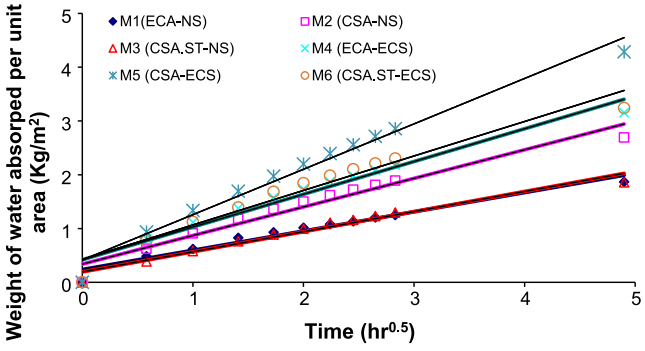

Fig. 20. Capillarity water absorption of concrete at 28 days.

Table 3, the LWAC produced with treated CSA showed better resistance to water penetration than that produced with ECA. This could be due to the microstructure of the interfacial transition zone (ITZ), between the aggregate and the cement matrix, which affects the mechanical properties and durability of concrete [51,52].

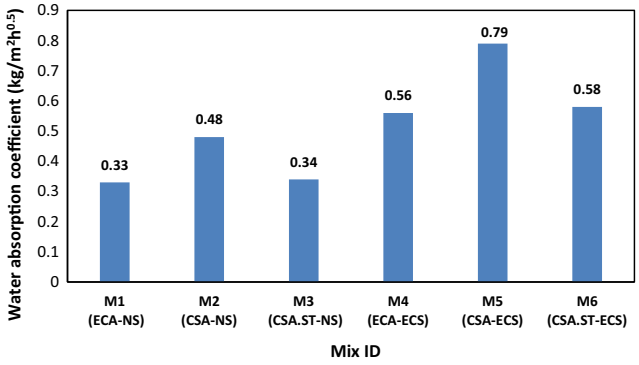

Fig. 21. Water capillarity coefficient of concrete.

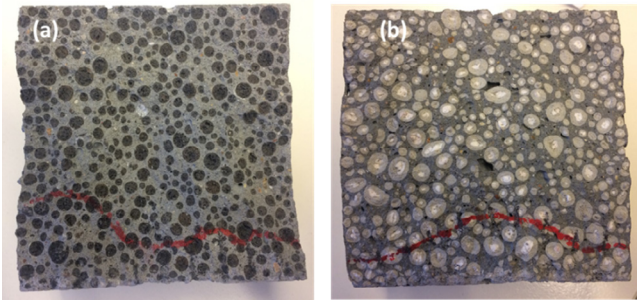

Fig. 22. Split samples after the water penetration test for (a) M1, (b) M2.

The microstructure of the ITZ between the cement matrix and CSA.ST and ECA are shown in Fig. 23a and b, respectively. A good and continuous bond between the CSA.ST and the cement matrix can be seen in Fig. 23a. The boundaries of CSA are therefore relatively indistinguishable, especially since both the CSA and the cement matrix have nearly the same composition. On the contrary, the boundaries of ECA can be clearly recognized in Fig. 23b, because of its microstructure, which is totally different from that of the cement matrix. It can be noticed that the ITZ surrounding CSA.ST is denser than that surrounding ECA. This may be attributable to the internal curing caused by the water stored within the aggregates [53]. Consequently, the amount of water reserved in CSA, which is much higher than that stored in ECA, contributed continuously to supplying the needed curing for the hydration of ITZ, thereby forming a homogeneous and dense transition zone. Here, it should be pointed out that sample

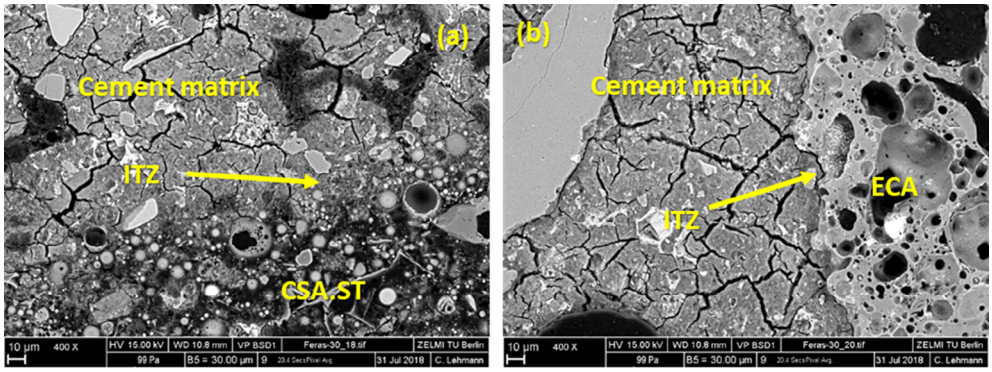

Fig. 23. SEM images of ITZ (a) for CSA.ST concrete, (b) for ECA concrete.

preparation was the main reason for the appearance of cracks in the cement matrix.

4. Conclusions

From the findings obtained in this experimental study, the following conclusions can be drawn:

- The cold bonding technique can be successfully employed to produce a new kind of cold-bonded LWA with low density, besides the possibility of producing different aggregate sizes.
- Core-shell LWAs in a size range of 2–4 mm and 4–8 mm were produced, having a particle density of 0.98 and 1 g/cm^3 and crushing strength of 3.11 and 3.54 MPa, respectively.
- Among the curing methods studied, curing at a relative humidity of 99% is the most suitable method to ensure the best crushing strength of CSA.
- The strength development of CSA showed a strong correlation with the results of SEM, TGA and XRD tests.
- The dry density of CSA concrete ranged from 1115 to 1540 kg/m^3. CSA are therefore feasible for the production of lightweight concrete with density classes from D1.2 to D1.6, as specified in EN 206-1.
- The compressive strength of CSA concrete ranged from 17.9 to 29.1 MPa and the thermal conductivity from 0.3169 to 0.666 W/m·K. This concrete can thus be classified as a structural and insulating concrete, with a higher thermal conductivity than ECA concrete.
- The incorporation of surface treated CSA increased the strength/density ratio and modulus of elasticity of CSA.ST concrete, as compared with ECA concrete.
- The water capillarity coefficient of LWAC made of CSA.ST, is comparable to that of ECA concrete, while the water penetration resistance is better.

The results of this study encourage development of the production and application of core-shell aggregate produced through cold bonding techniques, which may offer important economic and environmental benefits.

Conflict of interest

The authors declare no conflicts of interest.

Acknowledgments

The authors wish to thank the German Academic Exchange Service for their support (DAAD, Ref. no.: 91580050) in this research project.

References

[1] M. Aslam, P. Shafigh, M.Z. Jumaat, M. Lachemi, Benefits of using blended waste coarse lightweight aggregates in structural lightweight aggregate concrete, J. Clean. Prod. 119 (2016) 108–117, https://doi.org/10.1016/j.jclepro.2016.01.071.
[2] T.Y. Lo, W.C. Tang, H.Z. Cui, The effects of aggregate properties on lightweight concrete, Build. Environ. 42 (2007) 3025–3029, https://doi.org/10.1016/j.buildenv.2005.06.031.
[3] G. Joseph, K. Ramamurthy, Influence of fly ash on strength and sorption characteristics of cold-bonded fly ash aggregate concrete, Constr. Build. Mater. 23 (2009) 1862–1870, https://doi.org/10.1016/j.conbuildmat.2008.09.018.
[4] V.R.P. Kumar, K. Anandh, M. Kumar, An experimental study on partial replacement of natural coarse aggregate with fly ash coarse aggregate (FACA), Res. Appl. Sci. Eng. Technol. 2 (2014) 212–223.
[5] N.A. Libre, M. Shekarchi, M. Mahoutian, P. Soroushian, Mechanical properties of hybrid fiber reinforced lightweight aggregate concrete made with natural pumice, Constr. Build. Mater. 25 (2011) 2458–2464, https://doi.org/10.1016/j.conbuildmat.2010.11.058.
[6] L. Korat, V. Ducman, A. Legat, B. Mirtič, Characterisation of the pore-forming process in lightweight aggregate based on silica sludge by means of X-ray micro-tomography (micro-CT) and mercury intrusion porosimetry (MIP), Ceram. Int. 39 (2013) 6997–7005, https://doi.org/10.1016/j.ceramint.2013.02.037.
[7] Q.L. Yu, P. Spiesz, H.J.H. Brouwers, Ultra-lightweight concrete: conceptual design and performance evaluation, Cem. Concr. Compos. 61 (2015) 18–28, https://doi.org/10.1016/j.cemconcomp.2015.04.012.
[8] T.Y. Lo, H.Z. Cui, Z.G. Li, Influence of aggregate pre-wetting and fly ash on mechanical properties of lightweight concrete, Waste Manag. 24 (2004) 333–338, https://doi.org/10.1016/j.wasman.2003.06.003.
[9] G. Baykal, A.G. Döven, Utilization of fly ash by pelletization process; theory, application areas and research results, Resour. Conserv. Recycl. 30 (2000) 59–77, https://doi.org/10.1016/S0921-3449(00)00042-2.
[10] A. Terzić, L. Pezo, V. Mitić, Z. Radojević, Artificial fly ash based aggregates properties influence on lightweight concrete performances, Ceram. Int. 41 (2015) 2714–2726, https://doi.org/10.1016/j.ceramint.2014.10.086.
[11] P. Tang, M.V.A. Florea, H.J.H. Brouwers, Employing cold bonded pelletization to produce lightweight aggregates from incineration fine bottom ash, J. Clean. Prod. 165 (2017) 1371–1384, https://doi.org/10.1016/j.jclepro.2017.07.234.
[12] M. Gesoğlu, E. Güneyisi, S.F. Mahmood, H. Öznur Öz, K. Mermerdaş, Recycling ground granulated blast furnace slag as cold bonded artificial aggregate partially used in self-compacting concrete, J. Hazard. Mater. 235–236 (2012) 352–358, https://doi.org/10.1016/j.jhazmat.2012.08.013.
[13] J. Thomas, B. Harilal, Properties of cold bonded quarry dust coarse aggregates and its use in concrete, Cem. Concr. Compos. 62 (2015) 67–75, https://doi.org/10.1016/j.cemconcomp.2015.05.005.
[14] H. Chao-Lung, B. Le Anh-Tuan, C. Chun-Tsun, Effect of rice husk ash on the strength and durability characteristics of concrete, Constr. Build. Mater. 25 (2011) 3768–3772, https://doi.org/10.1016/j.conbuildmat.2011.04.009.
[15] N.U. Kockal, T. Ozturan, Strength and elastic properties of structural lightweight concretes, Mater. Des. 32 (2011) 2396–2403, https://doi.org/10.1016/j.matdes.2010.12.053.
[16] F. Tajra, M. Abd Elrahman, S.Y. Chung, D. Stephan, Performance assessment of core-shell structured lightweight aggregate produced by cold bonding pelletization process, Constr. Build. Mater. 179 (2018) 220–231, https://doi.org/10.1016/j.conbuildmat.2018.237.
[17] P. Gomathi, A. Sivakumar, Accelerated curing effects on the mechanical performance of cold bonded and sintered fly ash aggregate concrete, Constr. Build. Mater. 77 (2015) 276–287, https://doi.org/10.1016/j.conbuildmat.2014.12.108.
[18] M.S. Nadesan, P. Dinakar, Structural concrete using sintered flyash lightweight aggregate: a review, Constr. Build. Mater. 154 (2017) 928–944, https://doi.org/10.1016/j.conbuildmat.2017.08.005.

[19] S.Y. Chung, M.A. Elrahman, D. Stephan, P.H. Kamm, Investigation of characteristics and responses of insulating cement paste specimens with Aer solids using X-ray micro-computed tomography, Constr. Build. Mater. 118 (2016) 204–215, https://doi.org/10.1016/j.conbuildmat.2016.04.159.
[20] S.Y. Chung, T.S. Han, T.S. Yun, K.S. Youm, Evaluation of the anisotropy of the void distribution and the stiffness of lightweight aggregates using CT imaging, Constr. Build. Mater. 48 (2013) 998–1008, https://doi.org/10.1016/j.conbuildmat.2013.07.082.
[21] DIN EN 13055:2015-11: Leichte Gesteinskörnungen; Deutsche und Englische Fassung FprEN 13055:2015 – Anhang C: Bestimmung der Kornfestigkeit.
[22] K. Scrivener, R. Snellings, B. Lothenbach, A Practical Guide to Microstrucural Analysis of Cementitious Materials, Taylor & Francis, 2016.
[23] H.F.W. Taylor, Cement chemistry, Cem. Concr. Compos. 20 (1998) 335, https://doi.org/10.1016/S0958-9465(98)00023-7.
[24] T. Hemalatha, M. Mapa, N. George, S. Sasmal, Physico-chemical and mechanical characterization of high volume fly ash incorporated and engineered cement system towards developing greener cement, J. Clean. Prod. 125 (2016) 268–281, https://doi.org/10.1016/j.jclepro.2016.03.118.
[25] O. Sengul, S. Azizi, F. Karaosmanoglu, M.A. Tasdemir, Effect of expanded perlite on the mechanical properties and thermal conductivity of lightweight concrete, Energy Build. 43 (2011) 671–676, https://doi.org/10.1016/j.enbuild.2010.11.008.
[26] O. Youssf, R. Hassanli, J.E. Mills, M. Abd Elrahman, An experimental investigation of the mechanical performance and structural application of LECA-Rubcrete, Constr. Build. Mater. 175 (2018) 239–253, https://doi.org/10.1016/j.conbuildmat.2018.04.184.
[27] S.K.T. Khafaji, E.A. Al-Majed, Synthesis of Light expanded clay aggregates from Iraqi raw materials, IJSER 7 (2016) 690–696.
[28] DIN EN 1097-3-1998: Prüfverfahren für mechanische und physikalische Eigenschaften von Gesteinskörnungen – Teil 3: Bestimmung von Schüttdichte und Hohlraumgehalt.
[29] F. Tajra, M.A. Elrahman, D. Stephan. An experimental study of using core-shell structured lightweight aggregate in producing lightweight concrete. International Conference on Sustainable, Environmental Friendly Construction Materials, ICSEFCM, 2018, pp. 35–40.
[30] H.K. Kim, J.H. Jeon, H.K. Lee, Workability, and mechanical, acoustic and thermal properties of lightweight aggregate concrete with a high volume of entrained air, Constr. Build. Mater. 29 (2012) 193–200, https://doi.org/10.1016/j.conbuildmat.2011.08.067.
[31] DIN EN 12390-1-2012: Prüfung von Festbeton – Teil 1: Form, Maße und andere Anforderungen für Probekörper und Formen; Deutsche Fassung EN 12390-1:2012.
[32] DIN EN 12350-5-2009: Prüfung von Frischbeton – Teil 5: Ausbreitmaß; Deutsche Fassung EN 12350-5:2009.
[33] DIN EN 12390-7-2009: Prüfung von Festbeton – Teil 7: Dichte von Festbeton; Deutsche Fassung EN 12390-7:2009.
[34] DIN EN 12390-3-2009: Prüfung von Festbeton – Teil 3: Druckfestigkeit von Probekörpern; Deutsche Fassung EN 12390-3:2009.
[35] DIN EN 1048-5-2009: Prüfverfahren für Beton, Festbeton, gesondert hergestellte Probekörper.
[36] DIN EN ISO 15148-2001: Bestimmung des Wasseraufnahmekoeffizienten bei teilweisem Eintauchen; Deutsche Fassung EN ISO 15148:2002.
[37] DIN EN 206-1-2000: Beton – Teil 1: Festlegung, Eigenschaften, Herstellung und Konformität; Deutsche Fassung EN 206-1:2001.
[38] H.Z. Cui, T.Y. Lo, S.A. Memon, W. Xu, Effect of lightweight aggregates on the mechanical properties and brittleness of lightweight aggregate concrete, Constr. Build. Mater. 35 (2012) 149–158, https://doi.org/10.1016/j.conbuildmat.2012.02.053.
[39] J.-I. Sim, K.-H. Yang, E.-T. Lee, S.-T. Yi, Effects of aggregate and specimen sizes on lightweight concrete fracture energy, J. Mater. Civ. Eng. 26 (2014) 845–854, https://doi.org/10.1061/(ASCE)MT.1943-5533.0000884.
[40] ACI Committee 213R-03, Guide for Structural Lightweight Aggregate Concrete, American Concrete Institute, 2003.
[41] M. Bhattacharjee, Effect of aggregate properties on the crushing strength of concrete, Int. J. Mater. Sci. Appl. 4 (2015) 343, https://doi.org/10.11648/j.ijmsa.20150405.19.
[42] Y. Ke, A.L. Beaucour, S. Ortola, H. Dumontet, R. Cabrillac, Influence of volume fraction and characteristics of lightweight aggregates on the mechanical properties of concrete, Constr. Build. Mater. 23 (2009) 2821–2828, https://doi.org/10.1016/j.conbuildmat.2009.02.038.
[43] G. Joseph, K. Ramamurthy, Workability and strength behaviour of concrete with cold-bonded fly ash aggregate, Mater. Struct. Constr. 42 (2009) 151–160, https://doi.org/10.1617/s11527-008-9374-x.
[44] T.Y. Lo, H. Cui, S.A. Memon, T. Noguchi, Manufacturing of sintered lightweight aggregate using high-carbon fly ash and its effect on the mechanical properties and microstructure of concrete, J. Clean. Prod. 112 (2016) 753–762, https://doi.org/10.1016/j.jclepro.2015.07.001.
[45] A.M. Neville, Properties of Concrete, John Wiley & Sons, 2004.
[46] N.U. Kockal, T. Ozturan, Effects of lightweight fly ash aggregate properties on the behavior of lightweight concretes, J. Hazard. Mater. 179 (2010) 954–965, https://doi.org/10.1016/j.jhazmat.2010.03.098.
[47] I.B. Topçu, T. Uygunoğlu, Effect of aggregate type on properties of hardened self-consolidating lightweight concrete (SCLC), Constr. Build. Mater. 24 (2010) 1286–1295, https://doi.org/10.1016/j.conbuildmat.2009.12.007.
[48] H. Oktay, R. Yumrutaş, A. Akpolat, Mechanical and thermophysical properties of lightweight aggregate concretes, Constr. Build. Mater. 96 (2015) 217–225, https://doi.org/10.1016/j.conbuildmat.2015.08.015.
[49] I. Asadi, P. Shafigh, Z.F. Bin Abu Hassan, N.B. Mahyuddin, Thermal conductivity of concrete – a review, J. Build. Eng. 20 (2018) 81–93, https://doi.org/10.1016/j.jobe.2018.07.002.
[50] Y.G. Zhu, S.C. Kou, C.S. Poon, J.G. Dai, Q.Y. Li, Influence of silane-based water repellent on the durability properties of recycled aggregate concrete, Cem. Concr. Compos. 35 (2013) 32–38, https://doi.org/10.1016/j.cemconcomp.2012.08.008.
[51] T.Y. Lo, H.Z. Cui, Effect of porous lightweight aggregate on strength of concrete, Mater. Lett. 58 (2004) 916–919, https://doi.org/10.1016/j.matlet.2003.07.036.
[52] X. Sun, B. Zhang, Q. Dai, X. Yu, Investigation of internal curing effects on microstructure and permeability of interface transition zones in cement mortar with SEM imaging, transport simulation and hydration modeling techniques, Constr. Build. Mater. 76 (2015) 366–379, https://doi.org/10.1016/j.conbuildmat.2014.12.014.
[53] D.P. Bentz, Influence of internal curing using lightweight aggregates on interfacial transition zone percolation and chloride ingress in mortars, Cem. Concr. Compos. 31 (2009) 285–289, https://doi.org/10.1016/j.cemconcomp.2009.03.001.